Electronic Supplementary Material (ESI) for Nanoscale.
This journal is © The Royal Society of Chemistry 2019

Layer-dependent dielectric and optical properties of centimeter-scale 2D WSe_2: Evolution from a single layer to few layers (Supporting Information)

Honggang Gu,[‡a] Baokun Song,[‡a] Mingsheng Fang,[a] Yilun Hong,[b] Xiuguo Chen,[a] Hao Jiang,[a] Wencai Ren,[*b] and Shiyuan Liu[*]a

[a]State Key Laboratory of Digital Manufacturing Equipment and Technology, Huazhong University of Science and Technology, Wuhan 430074, Hubei, China.
E-mail: shyliu@hust.edu.cn

[b]Shenyang National Laboratory for Materials Science Institute of Metal Research Chinese Academy of Sciences, Shenyang 110016, P. R. China.
E-mail: wcren@imr.ac.cn

‡These authors contributed equally to the work.

XPS

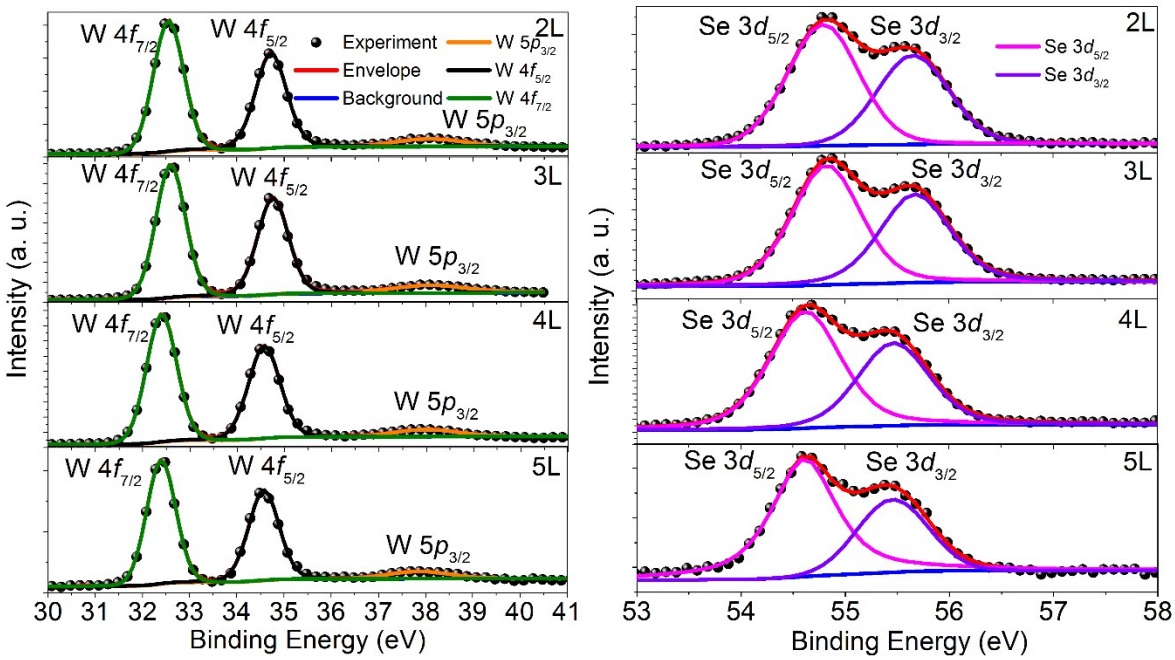

Fig. S1 Measured XPS spectra and corresponding peak-differentiation-imitating analysis results of 2–5 layer (L) WSe_2 films.

AFM

The surface roughness and thicknesses of 2–5L WSe_2 specimens are measured by AFM (Fig. S2, Table S1). The areas enclosed by the white dashed boxes are 1μm × 1μm, which are used to evaluate the surface roughness of WSe_2 films.

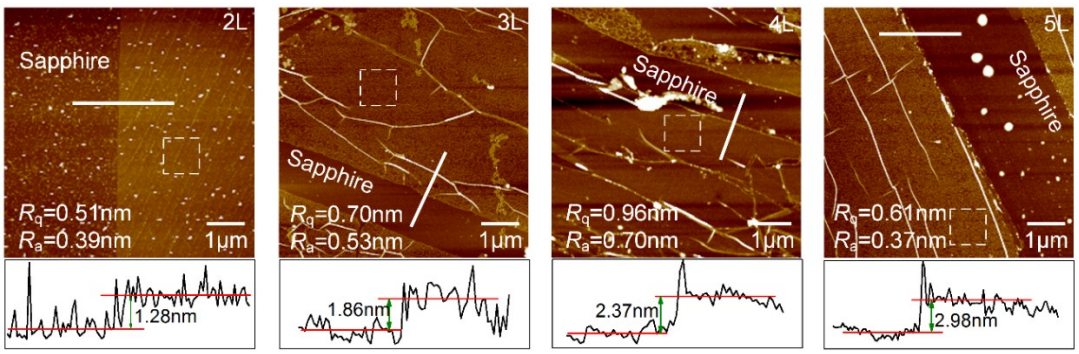

Fig. S2 AFM image of 2–5L WSe_2, and the high profiles across the white solid lines.

Raman Spectra

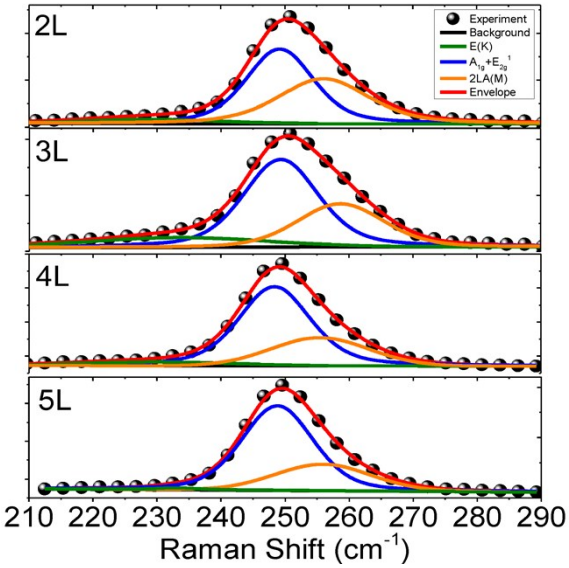

Fig. S3 Raman spectra of 2–5L WSe_2 films, the wavelength of the detection laser is 532 nm.

Ellipsometric analysis

Ellipsometry is a model-based technique. To analyze the measured ellipsometric spectra, two models need to be constructed, namely the optical model (Fig. 2a) and the dielectric function model. The optical model describes the light propagation through the optical stack of the sample calculated by the optical interference theory in multilayer films. While the dielectric function model gives the dispersion properties of the material which would be involved in the optical model. The 2D WSe_2 fabricated by us can be treated as the optical uniaxial material due to the vertical stratified microstructure resulting from the transferring process. The dielectric properties of the 2D WSe_2 can be described by a dielectric tensor

$$\boldsymbol{\varepsilon}=\begin{bmatrix} \varepsilon_o & & \\ & \varepsilon_o & \\ & & \varepsilon_e \end{bmatrix}, \tag{S1}$$

where, $\varepsilon = \varepsilon_1 - i\varepsilon_2$ is the dielectric function, ε_1 and ε_2 are the real part and imaginary part. The subscripts 'o' and 'e' refer to the ordinary parameters and the extraordinary

parameters, respectively. The direction of ε_e is perpendicular to the surface of the 2D WSe_2 sample (parallel to z-axis) and ε_o lies in the surface of the 2D WSe_2 (x-o-y plane) (Fig. 2a). ε_o and ε_e are also called the in-plane dielectric function and the out-of-plane dielectric function. For the in-plane dielectric function ε_o of the 2D WSe_2, we use 5 Lorentz oscillators and 3 Cody-Lorentz oscillators to describe the dispersion properties. The specific expression is as follows

$$\varepsilon_{\mathrm{o}} = \sum_{m=1}^{M} \varepsilon_{\mathrm{Lorentz}}^{m}(A_m, \eta_m, E_{\mathrm{n}m}; E) + \sum_{q=1}^{Q} \varepsilon_{\mathrm{Cody\text{-}Lorentz}}^{q}(A_q, \eta_q, E_{\mathrm{n}q}, E_{\mathrm{g}q}, E_{\mathrm{t}q}, E_{\mathrm{p}q}, E_{\mathrm{u}q}; E), \tag{S2}$$

where, $\varepsilon_{\mathrm{Lorentz}}^{m}$ and $\varepsilon_{\mathrm{Cody\text{-}Lorentz}}^{q}$ are the Lorentz oscillator model and the Cody-Lorentz oscillator model. They can be written as

$$\varepsilon_{\mathrm{Lorentz}}^{m}(E) = \frac{A_m \cdot \eta_m \cdot E}{E^2 - E_{\mathrm{n}m}{}^2 - \mathrm{i}E_{\mathrm{n}m} \cdot \eta_m}, \tag{S3}$$

$$\varepsilon_{\mathrm{Cody\text{-}Lorentz}}^{q}(E) = \varepsilon_{1q} - \mathrm{i}\varepsilon_{2q}, \tag{S4a}$$

$$\varepsilon_{2q}(E) = \begin{cases} \dfrac{E_{1q}}{E}\exp\left(\dfrac{E - E_{\mathrm{g}q} - E_{\mathrm{t}q}}{E_{\mathrm{u}q}}\right); & 0 < E < (E_{\mathrm{g}q} + E_{\mathrm{t}q}) \\ G(E)L(E) = \dfrac{(E - E_{\mathrm{g}q})^2}{(E - E_{\mathrm{g}q})^2 + E_{\mathrm{p}q}{}^2} \cdot \dfrac{A_q \cdot E_{\mathrm{n}q} \cdot \eta_q \cdot E}{(E^2 - E_{\mathrm{n}q}{}^2)^2 + \eta_q{}^2 \cdot E^2}; & (E_{\mathrm{g}q} + E_{\mathrm{t}q}) < E \end{cases}, \tag{S4b}$$

$$E_{1q} = (E_{\mathrm{g}q} + E_{\mathrm{t}q}) \cdot G(E_{\mathrm{g}q} + E_{\mathrm{t}q}) \cdot L(E_{\mathrm{g}q} + E_{\mathrm{t}q}). \tag{S4c}$$

Where, A, η, E_n refer to the amplitude, the damping coefficient, and the center energy of the oscillators. E_g is the bandgap energy, and E_t, E_p are the transition energies. E_u is the exponential rate of the Urbach absorption tail. $G(E)$ is the near-bandgap absorption function, which defines the Cody-absorption behavior, and $L(E)$ is the Lorentz oscillator function. The real part of the Cody-Lorentz oscillator can be calculated by the Kramer-Kroing relation (KKR). For the out-of-plane dielectric function ε_e of the 2D WSe_2, we use a Tauc-Lorentz oscillator model to embody the dispersion properties.[1] The expression of Tauc-Lorentz oscillator is

$$\varepsilon_{\text{Tauc-Lorentz}}(E) = \varepsilon_1 - \mathrm{i}\varepsilon_2, \tag{S5a}$$

$$\varepsilon_2(E) = \begin{cases} \dfrac{A \cdot \eta \cdot E_0 \cdot (E - E_g)^2}{(E^2 - E_n{}^2)^2 + \eta^2 E^2} \cdot \dfrac{1}{E}; & E > E_g \\ 0; & E \le E_g \end{cases}. \tag{S5b}$$

The real part of the Tauc-Lorentz oscillator can be calculated by KKR.

On the basic of the above models, the theoretical ellipsometric spectra of the 2D WSe_2 can be calculated. Fig. 2b and Fig. S4 illustrate the measured and best-fitting ellipsometric spectra of the 1-5L WSe_2. Obviously, the theoretical ellipsometric spectra are in good agreement with the experimental ellipsometric spectra.

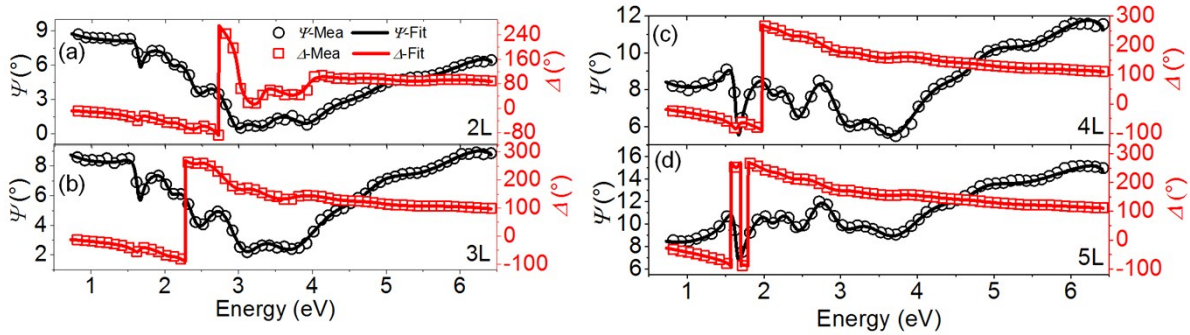

Fig. S4 Measured and best-matched ellipsometric spectra of 2–5L WSe_2 films.

Critical point analysis

To understand the physical mechanisms of the CPs showing in the in-plane dielectric fucntion spectra of the 2D WSe_2 films, CP analysis method is introduced to precisely determine the detailed parameters of the CPs. In the CP analysis, the second derivative of the in-plane dielectric function spectrum is fitted with the following theoretical formulas

$$\mathrm{d}^2\varepsilon_o / \mathrm{d}E^2 = \begin{cases} s(s-1)Amp \cdot \exp(\mathrm{i}\phi)(E - E_0 + \mathrm{i}\Gamma)^{s-2} & (s \ne 0) \\ Amp \cdot \exp(\mathrm{i}\phi)(E - E_0 + \mathrm{i}\Gamma)^{-2} & (s = 0) \end{cases}, \tag{S6}$$

here, Amp, ϕ, E_0, and Γ refer to the amplitude, the phase, the center energy, and the damping coefficient of the CP, and s stands for the dimension of the wave vector. Here, we set $s = -1$ to account for the excitonic behavior of the optical transitions occurring at these CPs.[2] The second derivatives of the in-plane dielectric functions and the best fitting curves (Fig. 4d and

Fig. S5d, h, l, p) show well consistency. The specific parameters in equation S6 to describe the CPs are listed in Table S2, and the values of E_0 are in agreement with previous experimental results[3,4] and theoretical predications.[5] Therefore, by means of the CP analysis method, both the positions and the shapes of these CPs in the 2D WSe_2 can be determined precisely.

Transitions of 2–5L WSe_2

According to the analysis method proposed by us, the physical origins of the transitions occurring at the CPs of 2–5L WSe_2 films can also be identified. The specific analysis results have been shown in Fig. S5. Comparing with the monolayer WSe_2, the physical origins of the CPs of 2–5L WSe_2 exhibit some subtle differences in the following aspects:

(1) For the 2–5L WSe_2, the valence band involved in the transitions of the CP E is V_1 rather than V_2.

(2) For the 2–5L WSe_2, the transition spatial position of the CP G in the Brillouin zone (BZ) is at Γ point rather than at K point.

The spin-orbit coupling and gradually prominent interlayer coupling in the 2–5L WSe_2 give rise to the above differences. The former induces the band splitting and redistribution, making the band structures of multilayer WSe_2 films more complex; the latter adjusts the relative positions of energy bands and changes the transition positions of these CPs in the BZ.

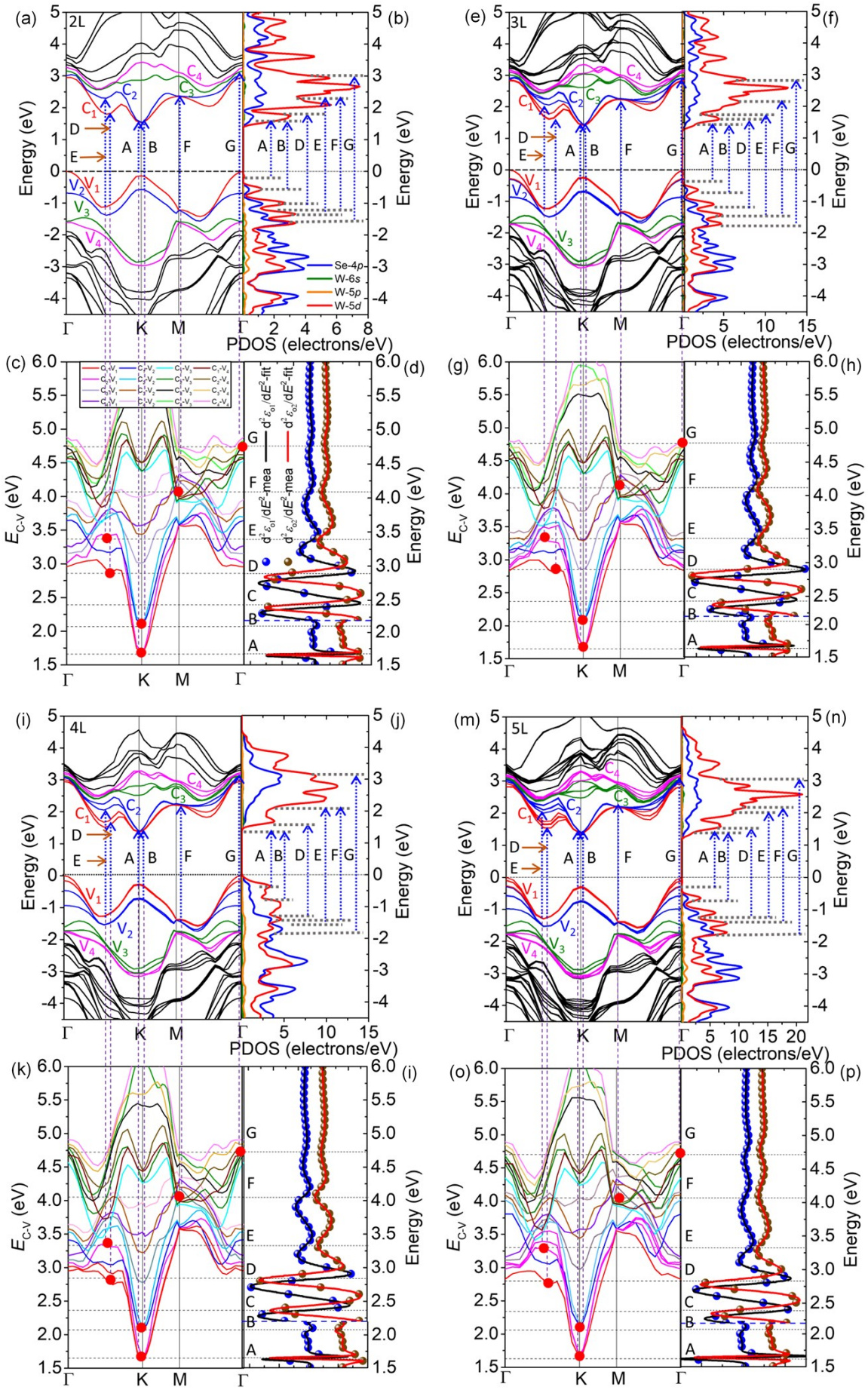
(a)
2L
(b)
(e)
3L
(f)
(c)
(d)
(g)
(h)
(i)
4L
(j)
(m)
5L
(n)
(k)
(l)
(o)
(p)
Energy (eV)
PDOS (electrons/eV)
E_{C-V} (eV)
Γ K M Γ
A B D E F G
Se-4p
W-6s
W-5p
W-5d

Fig. S5 (a, e, i, m) and (b, f, j, n): Band structures and projected density of state obtained from the first-principle calculations. (c, g, k, o) Energy differences between the first four conduction bands and the first four valence bands ($E_{C–V}$). (d, h, l, p) Critical point analysis results.

Table S1 summarized the thicknesses of the 1–5L WSe_2 determined by AFM and SE, and the thicknesses of the WSe_2 determined by different techniques agree well with each other. Table S2 lists the four parameters of equation S6, including the amplitude *Amp*, the phase ϕ, the center energy E_0, and the damping coefficient Γ. Table S3 and S4 list the in-plane and out-of-plane dielectric functions of 1–5L WSe_2.

Table S1 Thicknesses of 1–5L WSe_2 films determined by AFM and SE.

L	1	2	3	4	5
Thicknesses of AFM (nm)	0.75	1.28	1.86	2.37	2.98
Thicknesses of SE (nm)	0.62	1.15	1.83	2.40	3.11
Brugeman interlayer (nm)	0.40	0.21	0.55	0.50	0.54

Table S2 Summary of CP analysis results for 1–5L WSe_2 films.

Parameters	*Amp* (no unit)							*Φ* (°)						
CPs	A	B	C	D	E	F	G	A	B	C	D	E	F	G
1L	0.59	0.83	2.84	5.27	1.99	0.72	7.53	147.66	160.23	128.81	166.70	279.61	166.44	166.41
2L	0.45	0.73	2.16	4.32	2.69	3.04	1.53	147.60	160.22	128.80	217.08	179.23	147.57	135.50
3L	0.43	0.58	2.13	3.18	4.24	2.51	1.76	147.62	160.22	128.80	217.23	279.94	47.16	223.25
4L	0.47	0.47	2.26	3.66	5.02	2.21	3.01	147.44	160.26	128.83	217.26	279.94	47.07	223.34
5L	0.53	1.01	2.44	3.33	4.64	3.69	1.08	147.63	160.22	128.80	217.37	279.98	47.18	223.25
Parameters	E_0 (eV)							*Γ* (eV)						
CPs	A	B	C	D	E	F	G	A	B	C	D	E	F	G
1L	1.67	2.08	2.42	2.88	3.39	4.02	4.65	0.03	0.11	0.19	0.22	0.26	0.16	0.83
2L	1.66	2.07	2.39	2.86	3.37	4.07	4.74	0.04	0.14	0.17	0.24	0.32	0.45	0.46
3L	1.65	2.06	2.37	2.85	3.32	4.09	4.76	0.05	0.13	0.20	0.23	0.45	0.41	0.46
4L	1.65	2.07	2.36	2.84	3.33	4.05	4.72	0.05	0.11	0.21	0.26	0.47	0.37	0.58
5L	1.63	2.06	2.34	2.80	3.30	4.04	4.70	0.05	0.17	0.20	0.25	0.44	0.52	0.39

References

1 S. Funke, B. Miller, E. Parzinger, P. Thiesen, A. W. Holleitner, U. Wurstbauer, J. Phys.: Condens. Matter 2016, **28**, 385301.

2 W. Li, A. G. Birdwell, M. Amani, R. A. Burke, X. Ling, Y.-H. Lee, X. Liang, L. Peng, C. A. Richter, J. Kong, D. J. Gundlach, N. V. Nguyen, *Phys. Rev. B* 2014, **90**, 195434.

3 R. Frisenda, Y. Niu, P. Gant, A. J. Molina-Mendoza, R. Schmidt, R. Bratschitsch, J. Liu, L. Fu, D. Dumcenco, A. Kis, D. P. D. Lara, A. Castellanos-Gomez, *J. Phys. D: Appl. Phys.* 2017, **50**, 074002.

4 D. Kozawa, R. Kumar, A. Carvalho, K. K. Amara, W. Zhao, S. Wang, M. Toh, R. M. Ribeiro, A. H. C. Neto, K. Matsuda, G. Eda, *Nat. Commun.* 2014, **5**, 4543.

5 A. Ramasubramaniam, *Phys. Rev. B* 2012, **86**, 115409.